American Mineralogist, Volume 76, pages 1174–1183, 1991

Effect of Ti substitution in biotite-*1M* crystal chemistry

Maria Franca Brigatti*
Istituto di Chimica, Università della Basilicata, Potenza, Italy
Ermanno Galli
Istituto di Mineralogia e Petrologia, Università di Modena, Modena, Italy
Luciano Poppi
Dipartimento di Scienze Mineralogiche, Università di Bologna, Bologna, Italy

Abstract

Crystal structure refinements were performed on eight Ti-rich biotite-*1M* crystals from lamproitic rocks (Murcia and Albacete provinces, Spain), a monzonitic-alkali syenite pluton (Norway), an alkaline gabbro-peralkaline syenite association (Quebec, Canada), and a quartz diorite (Calabria, Italy). The refinements, carried out in space group *C*2/*m*, gave R values between 0.019 and 0.030. The crystals cover a Ti range from 0.29 to 1.05 atoms pfu (O + OH + F = 24) and a ratio of Mg/octahedral occupancy between 0.4 and 0.7. The structure refinements show the following: (1) In all samples the octahedral *trans* M1 site is larger and flatter than the *cis* M2 sites because of the preferential ordering of Fe plus Ti with respect to Mg. (2) The octahedral M1 site distortion increases as Ti increases and decreases as Mg/octahedral occupancy decreases. (3) For samples with Mg/octahedral occupancy >0.5, the refined occupancies of the M1 sites show that Ti^{4+} substitution is balanced by octahedral vacancies; M2 sites have features similar to those in Mg end-members because of the preferential ordering of Mg. (4) Octahedral sheet thickness in (Ti,Mg)-rich biotite is smaller than that in Fe-rich biotite.

Introduction

In trioctahedral *1M* micas, M1 and M2 octahedral sites can be occupied by the same kinds of cations (phlogopite = Mg end-member; annite = Fe end-member) or with different kinds of cations (biotite). In the first case, the geometry of the two sites should not change, whereas, in the second, the geometry depends on the nature of the site population.

Brigatti and Davoli (1990) analyzed biotite crystallized under different conditions and compared the structural parameters (distances, bond angles, and geometrical distortion parameters) with those reported in the literature for crystals on the trioctahedral *1M* join. They showed the following: (1) The trend of the octahedral sheet distortion is similar for M1 and M2 sites. As Fe content increases, the average distortion of the sheet decreases. (2) Biotite samples with few small, highly charged octahedral cations (Al, Ti, Fe) behave like those with many such cations.

The phenomenon of Ti substitution in natural biotite has been investigated by many authors (Guidotti et al., 1977; Dymek, 1983; Labotka, 1983). Nevertheless, there is still no agreement on the kind of substitution and on the crystallographic site occupied by Ti cations in the mica structure. Abrecht and Hewitt (1988), studying synthetic Ti-rich biotite, pointed out that the Ti-Tschermak substitution [$^{[6]}$Ti + 2 $^{[4]}$Al = $^{[6]}$(Mg,Fe) + 2 $^{[4]}$Si] may be the mechanism of Ti substitution in both iron and magnesium biotite, whereas the Ti-vacancies substitution [$^{[6]}$Ti + $^{[6]}\square$ = 2 $^{[6]}$(Fe,Mg)] is more important in magnesium biotite than in iron biotite. Unfortunately, the literature does not contain information on the variation of crystal chemical details and geometrical parameters in natural biotite samples resulting from the presence of Ti.

With the above in mind, this work reports a detailed crystal chemical study of eight biotite-*1M* samples with different Ti contents [0.29–1.05 atoms pfu, (O + OH + F) = 24] in order to verify preferential ordering of Ti, if any, and to determine how Ti substitution affects the crystal chemical features of the biotite structure, especially with regard to M1 and M2 octahedral sites.

Specimens studied

The occurrences of the eight biotite-*1M* samples are reported in Table 1. Samples 8–12 were from lamproitic volcanic rocks that occur as dikes and pungs in southeast Spain (Puebla de Mula, Fortuna, and Jumilla in Murcia province; Cancarix in Albacete province). Locality description, petrogenesis, and conditions of host rock crystallization are given in Venturelli et al. (1988). Sample 15 was from the alkaline gabbro and peralkaline syenite association of the Mont Saint Hilaire plutonic complex (Canada). Petrographic and geochemical details of the

*Present address: Istituto di Mineralogia e Petrologia, Università di Modena, L.go S. Eufemia, 19-41100 Modena, Italy.

0003–004X/91/0708–1174$02.00

Table 1. Sample numbers, host rocks, localities, original numbers, and donors of the biotite samples studied

Sample	Host rock	Locality	Original number	Donor
8	Lamproite	Puebla de Mula (Murcia prov., Spain)	Z3	1
9	Lamproite	Cancarix (Albacete prov., Spain)	Z2	1
10	Lamproite	Fortuna (Murcia prov., Spain)	Z4	1
11	Lamproite	Jumilla (Murcia prov., Spain)	Z8	1
12	Lamproite	Jumilla (Murcia prov., Spain)	Z9	1
15	Alkaline gabbro-peralkaline syenite	M. St. Hilaire (Quebec, Canada)	P1226a	2
16	Monzonite-alkali syenite	Sande cauldron (Oslo, Norway)	26	3
17	Quartz diorite	Capo Vaticano (Calabria, Italy)	38	4

Note: Donors are as follows: 1 = S. Capedri, Istituto di Mineralogia e Petrologia, Università di Modena, Italy. 2 = K.L. Currie, Geological Survey of Canada, Ottawa, Canada. 3 = T. Andersen, Mineralogisk-geologisk Museum, Norway. 4 = A. Rottura, Dipartimento di Scienze Mineralogiche, Università di Bologna, Italy.

pluton and the detailed mineral chemistry were studied by Currie et al. (1986). Sample 16 was from Sande cauldron, a monzonitic alkali syenite pluton (Oslo, Norway; Andersen, 1984). Sample 17 is from a quartz diorite (Capo Vaticano, Calabrian Arc, southern Italy) that occurs as minor intrusions in the upper part of a granulite-amphibolite facies metasedimentary sequence (Rottura et al., 1990).

Experimental details

Chemical analyses

Quantitative chemical analyses were obtained by an ARL-SEMQ electron microprobe for all crystals used in structure refinements.

Samples were analyzed by wavelength dispersive techniques using an accelerating potential of 15 kV, a sample current of 20 mA, and a defocused electron beam (spot size 3 μm). No volatilization of F was observed for counting times up to three times the routine counting times. Spectrometer data were reduced using the method of Ziebold and Ogilvie (1964) with correction factors of Albee and Ray (1970). The data (Table 2, the structural formulae are based on 24 O + F + OH) represent the averages of six to ten point analyses. The single crystals used in structure refinements showed high chemical homogeneity. However, according to the literature (Venturelli et al., 1984; Currie et al., 1986), biotite with different compositions was often found in most of the rock samples

Table 2. Chemical composition of biotites studied

	8	9	10	11	12	15	16	17
Biotite chemical composition								
SiO_3	39.31	40.13	39.00	38.70	39.38	36.41	36.32	36.14
Al_2O_3	15.94	12.80	13.09	14.70	13.06	14.38	13.95	15.85
TiO_2	2.64	3.26	9.25	5.83	4.83	6.89	3.97	3.44
Cr_2O_3	0.82	0.44	0.88	1.20	0.92	0.10	0.09	0.11
FeO*	6.42	4.63	9.33	8.14	8.05	15.00	19.18	20.26
MgO	20.00	22.45	14.31	17.20	19.00	13.18	12.16	10.92
MnO	0.36	0.22	0.49	0.44	0.27	0.36	0.35	0.14
Na_2O	0.11	0.17	0.11	0.21	0.18	0.10	0.13	0.15
K_2O	10.30	10.30	9.99	10.10	10.07	9.55	9.81	9.37
CaO	0.38	0.07	0.05	0.16	0.02	0.08	0.10	0.01
H_2O	2.82	2.40	1.10	2.00	2.30	3.55	2.65	3.52
F	0.86	3.13	2.40	1.30	1.89	0.30	1.29	0.09
Sum	99.96	100.00	100.00	99.98	99.97	99.90	100.00	100.00
Biotite structural formulae								
Si	5.715	5.816	5.863	5.735	5.807	5.468	5.616	5.526
Al	2.285	2.184	2.137	2.265	2.193	2.532	2.384	2.474
Sum	8.000	8.000	8.000	8.000	8.000	8.000	8.000	8.000
Al	0.447	0.003	0.183	0.304	0.077	0.014	0.159	0.383
Cr	0.094	0.050	0.105	0.141	0.107	0.012	0.011	0.013
Fe^{2+}	0.781	0.561	1.173	1.009	0.993	1.884	2.480	2.591
Mg	4.333	4.849	3.206	3.799	4.175	2.950	2.802	2.488
Mn	0.044	0.027	0.062	0.055	0.034	0.046	0.046	0.018
Ti	0.289	0.355	1.046	0.650	0.536	0.778	0.462	0.396
Sum	5.988	5.845	5.775	5.958	5.922	5.684	5.960	5.889
Ca	0.059	0.011	0.008	0.025	0.003	0.013	0.017	0.002
Na	0.031	0.048	0.032	0.060	0.051	0.029	0.039	0.044
K	1.910	1.904	1.916	1.910	1.894	1.830	1.935	1.828
Sum	2.000	1.963	1.956	1.995	1.948	1.872	1.991	1.874
OH	2.735	2.320	1.103	1.977	2.262	3.556	2.733	3.590
F	0.395	1.435	1.141	0.609	0.881	0.142	0.631	0.044
O	20.870	20.245	21.756	21.414	20.857	20.302	20.636	20.366
Sum	24.000	24.000	24.000	24.000	24.000	24.000	24.000	24.000

* FeO_{tot}.

TABLE 3. Crystallographic data for biotite single crystals: sample size, number of total and observed reflections, agreement factors, and lattice parameters

Sample	Dimensions (mm)	N_{all}	N_{obs}	R_{sym} ×100	R_{all} ×100	R_{obs} ×100	*a* (Å)	*b* (Å)	*c* (Å)	β (°)	Vol. (Å³)
8	0.19 × 0.15 × 0.04	459	436	2.9	3.2	2.5	5.317(1)	9.207(1)	10.232(2)	99.98(2)	493.3
9	0.33 × 0.13 × 0.03	599	492	2.3	3.0	2.2	5.306(1)	9.190(1)	10.163(1)	100.11(1)	487.8
10	0.17 × 0.08 × 0.03	346	291	3.6	2.7	2.2	5.322(1)	9.228(3)	10.102(1)	100.25(1)	488.1
11	0.20 × 0.13 × 0.03	496	461	2.9	2.1	1.9	5.315(1)	9.204(1)	10.168(1)	100.13(2)	489.6
12	0.20 × 0.16 × 0.03	586	449	2.9	3.4	2.1	5.314(1)	9.190(1)	10.160(3)	100.18(2)	488.3
15	0.13 × 0.09 × 0.01	512	361	3.0	3.9	2.3	5.329(1)	9.235(2)	10.190(3)	100.20(2)	493.5
16	0.27 × 0.27 × 0.02	558	470	3.2	3.8	3.0	5.333(1)	9.256(6)	10.186(4)	100.17(3)	494.9
17	0.17 × 0.11 × 0.03	494	429	3.4	4.1	2.6	5.323(1)	9.215(2)	10.210(2)	100.14(2)	493.0

Note: Esd's on the last significant digit are in parentheses. $R_{sym} = \Sigma_{hkl} \Sigma^{N}_{i=1} |I_{hkl_i} - I_{hkl}| / \Sigma_{hkl} \Sigma^{N}_{i=1} I_{hkl_i}$.

studied. It was not possible to obtain Fe^{2+}/Fe^{3+} ratio values for single crystals and so this important variable was not considered. OH content was obtained by means of thermogravimetric analysis (TG) on crystals from the same rock sample. A DuPont 990 thermal analyzer was used with about 2–3 mg of powder heated at a rate of 10 °C/min in Ar gas (flow rate 30 mL/min) to prevent Fe oxidation.

Single-crystal X-ray diffractometry

Single-crystal precession or Weissenberg photographs were taken of at least eight crystals from the same rock sample to determine crystal perfection and the polytypes present. The best crystal found in each sample was used to determine cell dimensions and diffraction intensities. Each crystal was mounted along the *b* axis on an automated CAD4 (Enraf-Nonius) single-crystal diffractometer (Mo$K\alpha$ radiation and flat graphite crystal monochromator).

Cell dimensions were refined using the 2θ values for 25 centered reflections with $15° < \theta < 25°$. About 1600 intensities for reflections ($\pm h$, $\pm k$, l) were collected for $2° \leq \theta \leq 30°$ (l starting from $l = 0$).

Because the ($\Delta\omega$, $\Delta\theta$) plots (Einstein, 1974) show a vertical line in the $\Delta\omega$ direction because of the crystal mosaics, the ω scan mode was chosen (scan widths 4–6° in ω, a detector horizontal aperture between 0.3 and 0.8°; Davoli, 1989; Brigatti and Davoli, 1990) to ensure that full intensity was recorded. Three standard reflections measured every 3 h showed no significant intensity variation. Intensities were corrected for Lorentz and polarization factors. Absorption corrections were made by the semiempirical ψ-scan technique of North et al. (1968). Equivalent reflections were averaged and the resulting discrepancy factor (R_{sym}) was calculated.

Structural refinement

Crystal structure refinements were computed with the least-squares program ORFLS (Busing et al., 1962), as modified at the Centro di Studio per la Cristallografia Strutturale of Pavia. Appropriate fully ionized scattering factors were used for octahedral M1 and M2 and ditrigonal K sites; mixed scattering factors were assumed for anion sites (O/O^{2-}) and for tetrahedral sites (75% Si 25% Al^{3+})/(75% Si^{4+} 25% Al^{3+}).

As the distortion of the octahedral sites causes considerable variation in the arrangement of atoms from cell to cell, the interpretation of structural data is based on an average $C2/m$ structure. All the refinements started with the atomic coordinates of sample M73 in Brigatti and Davoli (1990), using reflections with $I > 5\sigma I$ and varying the occupancy factors and thermal parameters alternatively during the refinement cycles.

Table 3 gives a summary of the X-ray and the refinement data. Table 4 gives crystallographic coordinates and equivalent isotropic and anisotropic temperature factors. Table 5 lists Fo and Fc values.[1] Table 6 reports the relevant bond distances, angles, and distortion polyhedral parameters. Table 7 gives electron numbers for M1, M2, and K sites obtained by structure refinement (XRef) and electron probe microanalysis (EPMA).

DISCUSSION

Chemical composition

The biotite-*1M* samples have compositions with remarkable substitutions in the octahedral sheet. MgO contents range from 10.92% to 22.45% (2.49 to 4.85 atoms pfu), the main octahedral substitutions being Fe and Ti. FeO contents range from 4.63% to 20.26% (0.56 to 2.59 atoms pfu), but in most cases the values also include Fe_2O_3. TiO_2 contents range from 2.64% to 9.25% (0.29 to 1.05 atoms pfu). Small substitutions include Cr_2O_3 (0.09% to 1.20%, 0.01 to 0.14 atoms pfu) and MnO (0.14% to 0.49%, 0.02 to 0.06 atoms pfu). The $^{[6]}Al^{3+}$ substitutions range from 0.01 to 0.45 atoms pfu. The tetrahedral site compositions range from $Si_{5.86}Al_{2.14}$ to $Si_{5.47}Al_{2.53}$ ($2.16 < Si/Al < 2.74$).

Because the interlayer charges are quite constant, charge balance requires that a lower Si/Al ratio in the tetrahedral sheet be compensated for by an increase in net positive charges in the octahedral sheet. This can be achieved by

[1] A copy of Table 5 may be ordered as Document AM-91-462 from the Business Office, Mineralogical Society of America, 1130 Seventeenth Street NW, Suite 330, Washington, DC 20036, U.S.A. Please remit $5.00 in advance for the microfiche.

TABLE 4. Crystallographic coordinates and equivalent isotropic and anisotropic temperature factors ($\times 10^4$) for biotite studied

Atom	x/a	y/b	z/c	B_{eq} (Å^2)	β_{11}*	β_{22}*	β_{33}*	β_{12}*	β_{13}*	β_{23}*
Sample 8										
O(1)	0.0171(7)	0.0	0.1697(3)	1.93(9)	205(14)	52(4)	41(4)	0	0(6)	0
O(2)	0.3256(4)	0.2311(3)	0.1692(2)	1.89(6)	167(9)	66(3)	41(2)	−25(5)	19(4)	−5(2)
O(3)	0.1313(4)	0.1673(3)	0.3914(2)	1.26(5)	118(7)	33(2)	34(2)	−1(4)	12(3)	1(2)
O(4)	0.1311(6)	0.5	0.3979(3)	1.33(8)	90(11)	41(4)	40(3)	0	14(5)	0
M2	0.0	0.3347(2)	0.5	1.41(3)	93(4)	44(2)	43(1)	0	13(2)	0
M1	0.0	0.0	0.5	1.03(4)	73(6)	25(2)	36(2)	0	13(3)	0
K	0.0	0.5	0.0	3.04(5)	275(8)	94(3)	72(2)	0	24(3)	0
T	0.0756(2)	0.1668(1)	0.2269(1)	1.12(2)	86(3)	32(1)	33(1)	1(2)	11(1)	−1(1)
Sample 9										
O(1)	0.0220(5)	0.0	0.1682(2)	1.79(6)	221(11)	42(3)	38(3)	0	13(4)	0
O(2)	0.3222(3)	0.2334(2)	0.1672(2)	1.83(4)	157(6)	68(2)	38(2)	−20(3)	19(3)	−5(2)
O(3)	0.1309(3)	0.1672(2)	0.3911(2)	1.20(3)	98(5)	39(2)	30(1)	0(3)	7(2)	−2(2)
O(4)	0.1317(4)	0.5	0.4006(2)	1.11(5)	88(8)	33(3)	31(2)	0	7(3)	0
M2	0.0	0.3353(1)	0.5	1.25(2)	89(3)	42(1)	35(1)	0	10(1)	0
M1	0.0	0.0	0.5	1.38(3)	108(5)	37(2)	43(2)	0	16(2)	0
K	0.0	0.5	0.0	2.86(4)	257(5)	87(2)	71(1)	0	22(2)	0
T	0.0753(1)	0.1668(1)	0.2258(1)	1.01(1)	90(2)	28(1)	28(1)	−1(1)	10(1)	−1(1)
Sample 10										
O(1)	0.0291(8)	0.0	0.1673(5)	2.0(1)	246(19)	34(5)	47(5)	0	2(8)	0
O(2)	0.3187(5)	0.2368(3)	0.1663(3)	1.8(7)	149(10)	64(4)	39(3)	−20(6)	5(4)	−3(3)
O(3)	0.1321(4)	0.1687(3)	0.3907(3)	1.17(7))	100(10)	22(3)	42(3)	−4(6)	9(5)	−1(3)
O(4)	0.1308(7)	0.5	0.4007(4)	1.1(1)	65(15)	30(5)	45(5)	0	26(7)	0
M2	0.0	0.3398(2)	0.5	1.26(4)	71(5)	38(2)	44(2)	0	13(2)	0
M1	0.0	0.0	0.5	1.20(6)	81(8)	22(3)	50(3)	0	13(4)	0
K	0.0	0.5	0.0	2.65(6)	235(9)	70(3)	75(3)	0	19(4)	0
T	0.0743(2)	0.1670(1)	0.2232(1)	1.01(3)	67(4)	20(1)	40(1)	−1(3)	8(2)	−1(2)
Sample 11										
O(1)	0.0212(5)	0.0	0.1683(2)	1.57(6)	188(9)	35(3)	35(2)	0	4(4)	0
O(2)	0.3230(3)	0.2327(2)	0.1674(2)	1.58(4)	126(5)	62(2)	33(2)	−23(3)	17(2)	−6(2)
O(3)	0.1310(3)	0.1676(2)	0.3911(2)	0.97(3)	78(5)	29(2)	28(1)	1(3)	10(2)	−1(2)
O(4)	0.1312(4)	0.5	0.3998(2)	0.99(5)	75(7)	28(3)	31(2)	0	13(3)	0
M2	0.0	0.3364(1)	0.5	1.18(2)	70(3)	42(1)	34(1)	0	10(1)	0
M1	0.0	0.0	0.5	1.08(3)	80(4)	27(1)	38(1)	0	15(2)	0
K	0.0	0.5	0.0	2.67(3)	222(5)	80(2)	72(2)	0	22(2)	0
T	0.0749(1)	0.1669(1)	0.2255(1)	0.81(1)	62(2)	22(1)	26(1)	0(1)	9(1)	0(1)
Sample 12										
O(1)	0.0214(5)	0.0	0.1686(3)	1.91(6)	202(10)	53(3)	43(3)	0	14(4)	0
O(2)	0.3225(3)	0.2330(2)	0.1677(2)	1.88(4)	138(6)	72(3)	44(2)	−25(3)	21(3)	−4(2)
O(3)	0.1307(3)	0.1674(2)	0.3910(2)	1.31(4)	81(5)	48(2)	36(2)	1(3)	12(2)	−1(2)
O(4)	0.1311(4)	0.5	0.3995(2)	1.31(5)	70(7)	49(3)	39(2)	0	14(3)	0
M2	0.0	0.3357(1)	0.5	1.42(2)	79(3)	54(1)	40(1)	0	15(1)	0
M1	0.0	0.0	0.5	1.41(3)	85(4)	46(2)	45(2)	0	17(2)	0
K	0.0	0.5	0.0	2.98(4)	239(5)	93(2)	80(2)	0	27(2)	0
T	0.0750(1)	0.1668(1)	0.2258(1)	1.13(1)	71(2)	38(1)	34(1)	1(1)	11(1)	1(1)
Sample 15										
O(1)	0.0174(7)	0.0	0.1691(4)	1.68(9)	194(14)	33(4)	43(4)	0	7(6)	0
O(2)	0.3243(4)	0.2311(3)	0.1678(2)	1.60(6)	145(8)	56(3)	33(2)	−10(5)	18(4)	−7(2)
O(3)	0.1307(4)	0.1683(3)	0.3910(2)	0.99(5)	90(8)	29(2)	24(2)	−6(5)	4(3)	4(3)
O(4)	0.1293(6)	0.5	0.3964(3)	1.15(9)	108(14)	34(4)	28(4)	0	10(6)	0
M2	0.0	0.3368(1)	0.5	0.93(2)	64(3)	28(1)	27(1)	0	6(2)	0
M1	0.0	0.0	0.5	0.91(4)	88(6)	19(2)	29(2)	0	15(3)	0
K	0.0	0.5	0.0	2.74(5)	236(7)	73(3)	78(3)	0	22(4)	0
T	0.0742(1)	0.1671(1)	0.2250(1)	0.81(2)	76(3)	19(1)	24(1)	0(2)	8(1)	−1(1)
Sample 16										
O(1)	0.0297(8)	0.0	0.1678(4)	2.5(1)	283(17)	36(4)	74(5)	0	10(7)	0
O(2)	0.3201(5)	0.2368(3)	0.1678(3)	2.40(7)	202(9)	66(3)	65(3)	−27(5)	8(4)	−2(3)
O(3)	0.1310(4)	0.1679(3)	0.3905(2)	1.45(5)	112(7)	32(2)	50(2)	0(4)	13(3)	−1(2)
O(4)	0.1291(6)	0.5	0.3952(4)	1.75(8)	155(12)	43(4)	48(4)	0	−2(6)	0
M2	0.0	0.3355(1)	0.5	1.55(2)	97(3)	46(1)	50(1)	0	8(1)	0
M1	0.0	0.0	0.5	1.41(3)	112(5)	30(2)	49(2)	0	10(2)	0
K	0.0	0.5	0.0	3.72(6)	267(8)	92(3)	124(3)	0	25(4)	0
T	0.0747(1)	0.1669(1)	0.2254(1)	1.30(2)	78(3)	26(1)	53(1)	3(2)	10(1)	0(1)
Sample 17										
O(1)	0.0145(8)	0.0	0.1712(5)	2.5(1)	188(15)	49(5)	98(6)	0	35(7)	0
O(2)	0.3249(5)	0.2298(3)	0.1697(3)	2.42(7)	132(9)	64(4)	93(4)	−8(5)	36(4)	1(3)
O(3)	0.1302(4)	0.1671(3)	0.3904(2)	0.92(5)	66(7)	33(3)	23(2)	−14(4)	14(3)	8(2)
O(4)	0.1293(7)	0.5	0.3954(3)	1.17(8)	162(13)	45(4)	4(3)	0	0(5)	0
M2	0.0	0.3327(1)	0.5	0.90(2)	75(3)	22(1)	31(1)	0	20(1)	0
M1	0.0	0.0	0.5	0.97(3)	73(5)	23(2)	33(2)	0	10(2)	0
K	0.0	0.5	0.0	3.22(6)	212(8)	95(3)	106(3)	0	50(4)	0
T	0.0759(1)	0.1664(1)	0.2268(1)	1.02(2)	56(3)	33(1)	35(1)	−2(2)	20(1)	1(1)

Note: Esd's on the last significant digit are in parentheses.
* The terms refer to $e^{(-(h^2\beta_{11} + \cdots + 2hk\beta_{12} + \cdots))}$.

Table 6. Selected data from structure refinements of biotite samples

	8	9	10	11	12	15	16	17
T-O(1) (Å)	1.653(2)	1.648(1)	1.644(2)	1.649(1)	1.646(1)	1.654(2)	1.654(2)	1.648(2)
T-O(2) (Å)	1.655(2)	1.650(2)	1.645(3)	1.652(2)	1.650(2)	1.656(2)	1.658(3)	1.646(3)
T-O(2') (Å)	1.652(2)	1.649(2)	1.640(3)	1.648(2)	1.648(2)	1.650(3)	1.644(3)	1.663(3)
T-O(3) (Å)	1.657(2)	1.654(2)	1.665(3)	1.658(2)	1.652(2)	1.665(2)	1.655(3)	1.645(2)
⟨T-O⟩ (Å)	1.654	1.650	1.649	1.652	1.649	1.656	1.653	1.650
TQE	1.0004	1.0005	1.0002	1.0004	1.0004	1.0002	1.0003	1.0002
α (°)	7.46	6.56	5.23	6.84	6.72	7.46	5.23	7.97
Δz (Å)	0.005	0.010	0.010	0.009	0.009	0.013	0.000	0.015
τ (°)	110.54	110.72	110.03	110.52	110.53	110.17	110.46	110.12
M1-O(3) (×4) (Å)	2.090(2)	2.083(2)	2.100(3)	2.089(2)	2.085(2)	2.100(2)	2.103(3)	2.093(2)
M1-O(4) (×2) (Å)	2.057(3)	2.036(2)	2.041(4)	2.044(2)	2.044(2)	2.068(3)	2.076(3)	2.072(4)
⟨M1-O⟩ (Å)	2.079	2.067	2.081	2.074	2.071	2.089	2.094	2.086
OQE	1.0112	1.0131	1.0154	1.0130	1.0127	1.0117	1.0108	1.0097
ψ (°)	58.94	59.22	59.59	59.23	59.16	59.03	58.88	58.66
e_o/e_s	1.10593	1.11379	1.12336	1.11379	1.11241	1.10888	1.10460	1.09888
M2-O(3) (×2) (Å)	2.089(2)	2.089(2)	2.117(3)	2.097(2)	2.091(2)	2.101(3)	2.101(3)	2.082(3)
M2-O(3') (×2) (Å)	2.080(2)	2.074(2)	2.071(2)	2.076(1)	2.076(2)	2.082(2)	2.084(2)	2.086(2)
M2-O(4) (×2) (Å)	2.036(2)	2.012(2)	1.981(3)	2.010(2)	2.014(2)	2.029(3)	2.047(3)	2.062(2)
⟨M2-O⟩ (Å)	2.068	2.058	2.057	2.061	2.061	2.071	2.078	2.077
OQE	1.0104	1.0123	1.0138	1.0120	1.0118	1.0104	1.0095	1.0090
ψ (°)	58.76	59.07	59.20	59.02	58.99	58.73	58.62	58.51
e_o/e_s	1.10168	1.10989	1.11264	1.10814	1.10778	1.10074	1.09731	1.09479
K-O(1) (×2) (Å)	2.987(4)	2.988(3)	3.015(4)	2.989(3)	2.989(3)	2.981(4)	3.033(4)	2.978(4)
K-O(1') (×2) (Å)	3.340(4)	3.298(3)	3.262(5)	3.307(2)	3.308(3)	3.339(4)	3.275(4)	3.366(4)
K-O(2) (×4) (Å)	3.330(3)	3.285(2)	3.253(3)	3.297(2)	3.290(2)	3.321(3)	3.277(3)	3.337(3)
K-O(2') (×4) (Å)	2.990(3)	2.990(2)	3.017(3)	2.989(2)	2.991(2)	2.987(3)	3.038(3)	2.987(3)
K-O inner (Å)	2.989	2.989	3.016	2.989	2.990	2.985	3.036	2.984
K-O outer (Å)	3.333	3.289	3.256	3.300	3.296	3.327	3.276	3.347
Δ(K-O)* (Å)	0.344	0.300	0.240	0.311	0.306	0.342	0.240	0.363
t_{oct} (Å)	2.145	2.116	2.107	2.122	2.124	2.150	2.165	2.170
t_{tet} (Å)	2.264	2.272	2.265	2.265	2.257	2.255	2.254	2.230
t_{int} (Å)	3.405	3.346	3.305	3.358	3.363	3.369	3.354	3.421

Note: Entries in column 1 are: bond distances; TQE, OQE (Robinson et al., 1971); octahedral flattening angles ψ, tetrahedral rotation angles α (Hazen and Burnham, 1973); Δz = departure from coplanarity of the basal O atoms; tetrahedral flattening angles τ; e_o/e_s (Toraya, 1981). Esd's on the last significant digit are in parentheses.

* Refers to $\langle K\text{-}O_{outer}\rangle - \langle K\text{-}O_{inner}\rangle$.

an increase in Ti by the presence of $^{[6]}Al^{3+}$ or $^{[6]}Fe^{3+}$ or both.

Structural features: general considerations

In all the rock samples, both *1M* polytype and stacking disordered polytypes were present. In addition, *3T* and $2M_1$ polytypes were found in the lamproitic rocks.

In biotite crystals, the *a* and *b* parameters increase little as Fe or Ti content increases, whereas the *c* value tends to decrease as Ti increases. These trends (Tables 2 and 3) are particularly evident when the Mg-rich samples (8 to 12; $Mg/^{[6]}\Sigma > 0.5$, where $^{[6]}\Sigma$ is the octahedral occupancy) are considered separately from the Mg-poor samples (15 to 17; $Mg/^{[6]}\Sigma < 0.5$).

Micas with an average distance for ⟨M1-O⟩ greater than that for ⟨M2-O⟩ have β angles slightly larger than the ideal angle [$\beta_{ideal} = \arccos(-a/3c)$] observed when ⟨M1-O⟩ = ⟨M2-O⟩ (Bailey, 1975, 1984). For trioctahedral micas, the magnitude of this effect is approximately proportional to the size of the cations in M1 and M2. In the biotite examined, β is generally larger than β_{ideal}; hence, M1 must be larger than M2. In all samples, the differences between

Table 7. Mean atomic number of octahedral and interlayer sites as determined by structure refinement and microprobe analysis for biotite

	8	9	10	11	12	15	16	17
M1 XRef	13.87(4)	13.69(2)	16.33(8)	14.74(2)	14.53(2)	17.54(7)	19.05(4)	18.64(8)
M2 XRef	15.08(8)	13.99(5)	16.49(6)	16.77(5)	16.10(5)	17.0(1)	18.4(1)	18.4(1)
K XRef	19.21(5)	18.89(4)	18.64(6)	19.23(4)	18.66(4)	17.71(5)	19.04(6)	17.20(6)
M1 + M2 XRef*	44.03	41.67	49.31	48.29	46.74	51.54	55.84	55.43
M1 + M2 EPMA**	43.91	41.25	49.22	47.42	46.07	51.56	55.88	55.84
K EPMA	18.91	18.46	18.46	18.73	18.31	17.68	19.77	17.63

Note: Esd's on the last significant digit are in parentheses. XRef = X-ray refinement. EPMA = electron microprobe analysis.

* 2 × M2 + M1.

** Sum of octahedral cation electrons.

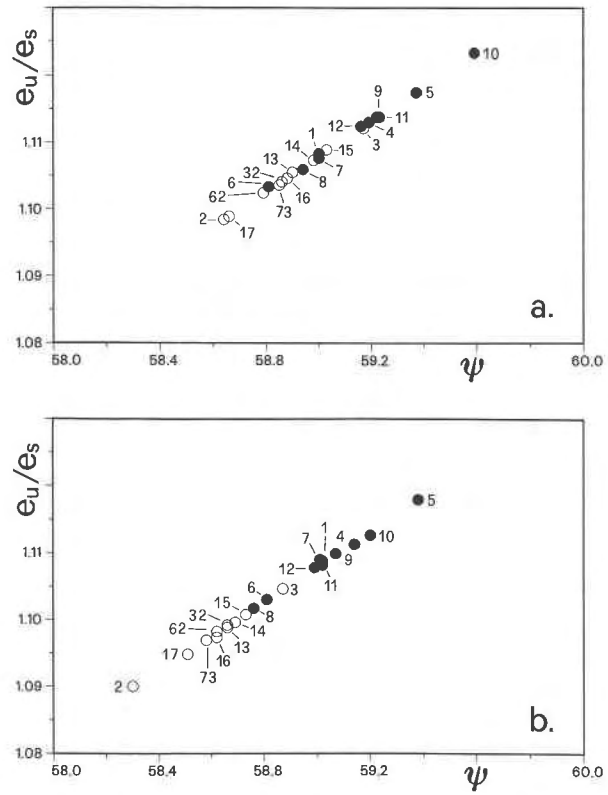

Fig. 1. Values of (e_u/e_s) vs. ψ (°) for M1 (**a**) and M2 (**b**) sites. Solid symbols = samples with $Mg/^{[6]}\Sigma > 0.5$; open symbols = samples with $Mg/^{[6]}\Sigma < 0.5$. Samples from this study = 8 to 12 and 15 to 17; samples from literature = 1 phlogopite (Hazen and Burnham, 1973), 2 annite (Hazen and Burnham, 1973), 3 biotite (Takeda and Ross, 1975), 4 phlogopite (Joswig, 1972), 5 fluorophlogopite (Takeda and Morosin, 1975), 6 phlogopite (Hazen et al., 1981), 7 fluorophlogopite (McCauley et al., 1973), 13, 14, 32, 62, 73 biotite (M13, M14, M32, M62, M73, respectively, in Brigatti and Davoli, 1990).

measured and calculated values are greater than the standard deviations.

The isotropic thermal factors (Table 4) are similar to those previously reported for trioctahedral micas (Takeda and Ross, 1975; Brigatti and Davoli, 1990). The tetrahedral atoms (T) have the lowest values and the interlayer atoms (K) the highest values, whereas the β_{eq} values of the M1 and M2 atoms are slightly higher than those of the tetrahedral sites. These observations are consistent with the crystal chemical nature of the sites (Vainshtein, 1981). The basal tetrahedral O atoms, O(1) and O(2), have higher isotropic thermal factors than O(3) and O(4). These larger isotropic temperature factors may result not only from crystallographic position but could also be affected by tetrahedral Si/Al disorder (Hazen and Burnham, 1973; Liebau, 1985).

In dioctahedral micas, which have vacant M1 sites, the OH dipole is nearly parallel to the (001) plane and points toward M1. In trioctahedral micas, the OH dipole is normal to the octahedral sheet, pointing toward the center of the six-membered ring of tetrahedra (Bailey, 1984). In a neutron refinement of phlogopite, Joswig (1972) located the H^+ at 1.003 Å from the O atom, with the OH vector normal to the (001) plane. At the end of our refinements, electron-density difference maps (ΔF) show maxima, which can be ascribed to H^+, only in samples 8 and 17 (probably owing to their higher OH content); the O-H separation is 0.87 Å for sample 8 (atomic coordinates for H, 0.10, 0.5, 0.318) and 1.05 Å for sample 17 (atomic coordinates for H, 0.02, 0.5, 0.315), with the OH vector in the first case almost parallel to **c*** and in the second, slightly divergent from **c***. The behavior of sample 17 can be linked to a partial ordering of the vacant sites of the octahedral sheet.

Octahedral sheet

Figures 1a and 1b show the relationships between (e_u/e_s) (the ratio between shared and unshared edge lengths, as in Toraya, 1981) and ψ (the octahedral flattening angle, as defined by Donnay et al., 1964; formula as in Hazen and Burnham, 1973) for the M1 and M2 sites, respectively. For both sites, as observed by Toraya (1981) and Brigatti and Davoli (1990), there is excellent correlation between the two variables [$r = 0.999$; regression equations: $(e_u/e_s)_{M1} = -0.4411 + 2.6253 \times 10^{-2} \times \psi_{M1}$ and $(e_u/e_s)_{M2} = -0.4371 + 2.6187 \times 10^{-2} \times \psi_{M2}$]. The following observations can be made: (1) In Mg end-members (samples 1 and 4), the average distortion of the octahedral sheet is greater than in Fe end-members (sample 2). (2) In Fe- and Ti-rich samples, distortion is greater in the M1 than in the M2 site. (3) In biotite with $Mg/^{[6]}\Sigma > 0.5$, the site distortion of M2 is comparable to that of Mg end-members, whereas it decreases when $Mg/^{[6]}\Sigma < 0.5$. (4) The increase in Ti content causes an increasing distortion in the M1 site that is even more evident when samples with $Mg/^{[6]}\Sigma > 0.5$ (samples 8, 9, 12, 11, 10, in that order) are considered separately from those with $Mg/^{[6]}\Sigma < 0.5$ (samples 17, 16, 15, in that order).

Figures 2a and 2b show the OQE (the octahedral quadratic elongation, Robinson et al., 1971) distortion trend vs. ψ for M1 and M2 sites, respectively. As expected, a trend similar to that in Figures 1a and 1b is observed, although the correlation is slightly lower ($r = 0.995$ and $r = 0.989$ for M1 and M2, respectively).

Figures 3a and 3b correlate average M1-O and M2-O distances with the distortion parameter OQE in M1 and M2 sites, respectively. The negative correlation holds for the M2 site [$r = -0.907$; regression equation: $\langle M2\text{-}O\rangle = 8.0823 - 5.9457 \times OQE$], whereas it is not so well developed for the M1 site ($r = 0.640$). In both sites, however, as already observed by Brigatti and Davoli (1990), an increase in distortion causes a faster decrease in the average distance $\langle M1\text{-}O\rangle$ than in that of $\langle M2\text{-}O\rangle$. Furthermore, the following relationships should be noted: (1) Samples with $Mg/^{[6]}\Sigma > 0.5$ and phlogopites fall into an area distinct from that of samples with $Mg/^{[6]}\Sigma < 0.5$. (2) Samples with $0.289 < Ti < 1.046$ atoms pfu and $Mg/^{[6]}\Sigma > 0.5$, with similar distortion values, have $\langle M2\text{-}O\rangle$ dis-

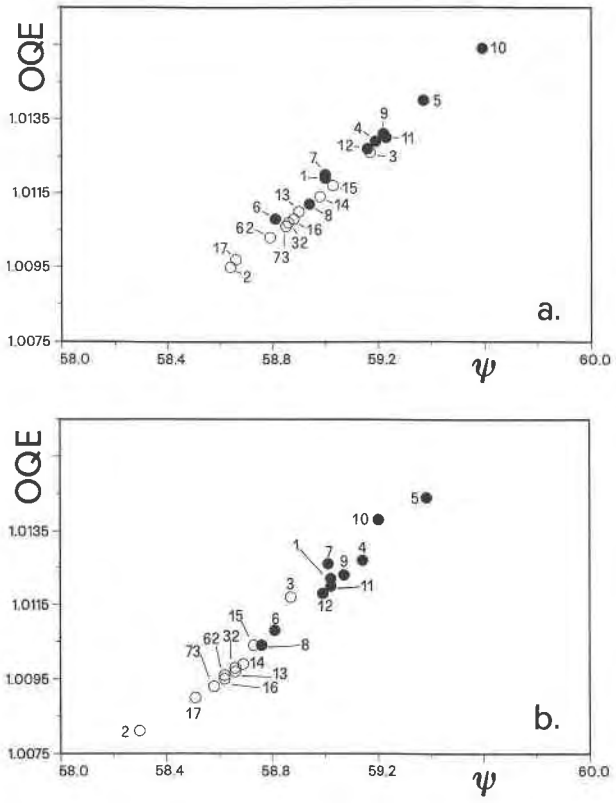

Fig. 2. OQE vs. ψ (°) for M1 (**a**) and M2 (**b**) sites. Symbols and samples as in Figure 1.

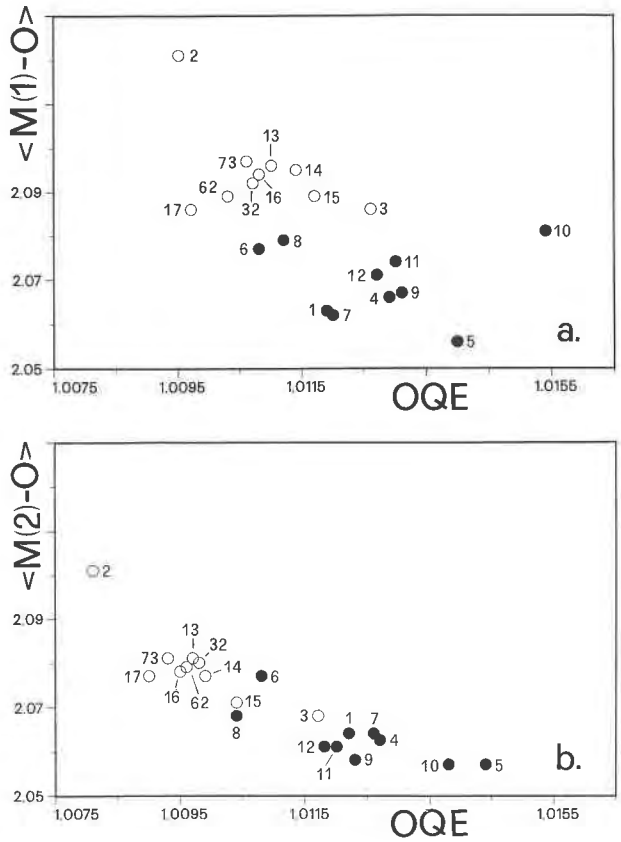

Fig. 3. Mean ⟨M-O⟩ distance (Å) vs. OQE for M1 (**a**) and M2 (**b**) sites. Symbols and samples as in Figure 1.

tances slightly smaller and ⟨M1-O⟩ distances slightly larger than Mg end-members (samples 1 and 4). (3) Sample 10, with the highest Ti content (Ti = 1.046 atoms pfu), has a markedly distorted M1 octahedron.

In Figure 4 $\Delta\langle$M-O$\rangle$ [$\Delta\langle$M-O$\rangle$ = ⟨M1-O⟩ − ⟨M2-O⟩] and $\Delta(e_u/e_s)$ [$\Delta(e_u/e_s) = (e_u/e_s)_{M1} - (e_u/e_s)_{M2}$] are correlated [$r = 0.988$; regression equation: $\Delta\langle\text{M-O}\rangle = 5.37 \times 10^{-4} + 2.2527 \times \Delta(e_u/e_s)$]. It can be seen that an increase in $\Delta\langle$M-O$\rangle$ causes an increase in the average distortion between the M1 and M2 octahedra. The differences between the two octahedra are generally smaller in the case of samples with $Mg/^{[6]}\Sigma > 0.5$ and larger in the case of samples with $Mg/^{[6]}\Sigma < 0.5$. Sample 10 (Ti = 1.040 atoms pfu) shows the largest variation, both in distortion and size, between the M1 and M2 octahedra.

Samples with $Mg/^{[6]}\Sigma > 0.5$ (samples from 8 to 12) have a smaller number of electrons in M1 and M2 sites ($41.67 < e_{(M1 + M2)} < 49.31$) than samples with $Mg/^{[6]}\Sigma < 0.5$ (samples from 15 to 17; $51.54 < e_{(M1 + M2)} < 55.84$), which is consistent with their chemical composition. Moreover, the number of electrons in the two sites differs, and M1 contains a slightly smaller number of electrons in samples with $Mg/^{[6]}\Sigma > 0.5$ and a greater number in the others (Table 7).

According to Weiss et al. (1985), large cations (or vacancies or both) tend to occupy the larger and flatter M1 octahedra.

The thickness of the octahedral sheet (t_{oct}) decreases when (Ti + Mg) in octahedral coordination increases ($r = -0.904$) (Fig. 5).

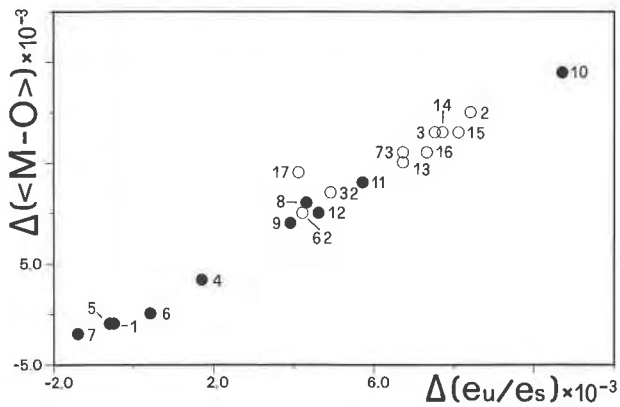

Fig. 4. Values of Δ(M-O) = (⟨M1-O⟩ − ⟨M2-O⟩) (Å) vs. $\Delta(e_u/e_s) = (e_u/e_s)_{M1} - (e_u/e_s)_{M2}$. Symbols and samples as in Figure 1.

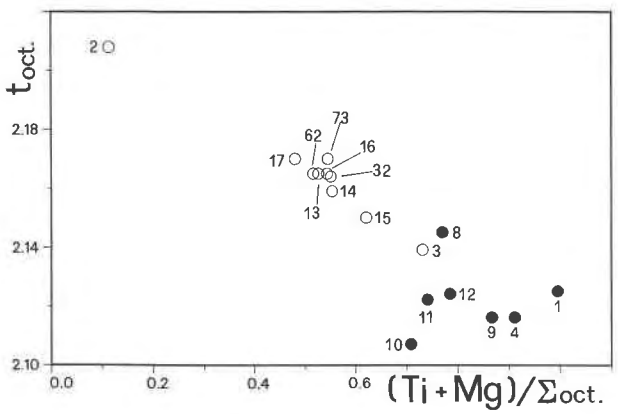

Fig. 5. Values of t_{oct} vs. (Ti + Mg)/$^{[6]}\Sigma$. Symbols and samples as in Figure 1.

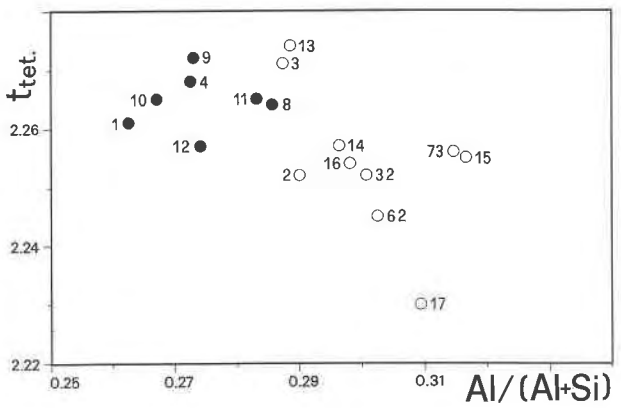

Fig. 6. Values of t_{tet} vs. Al/(Al + Si). Symbols and samples as in Figure 1.

Tetrahedral sheet

The average tetrahedron is very regular, as indicated by the tetrahedral distortion parameter TQE (tetrahedral quadratic elongation, Robinson et al., 1971) (from 1.0002 to 1.0005). The slight distortion involves elongation normal to (001) with τ (O_{apical}-T-O_{basal}) values (Table 6) in the range 110.03° to 110.72° (τ = 109.47° for an ideal tetrahedron). T-O bonds relative to apical O atoms are slightly larger than those relative to basal O atoms and the pyramidal edges are greater than the basal edges.

According to McKinney et al. (1988), substitution of a larger Al^{3+} for Si^{4+} increases the *a* and *b* dimensions of the tetrahedra and causes a reduction in the sheet thickness (t_{tet}) (Tables 2, 3, and 6). The Al fraction in the mica tetrahedra is usually deduced from the average ⟨T-O⟩ distance using the linear relationships in Hazen and Burnham (1973) or Abbott and Burnham (1988). The results of these determinations are generally lower than those given by chemical analysis (Table 8). Liebau (1985) hypothesized that high temperature factors, whether reflecting static disorder (e.g., caused by Si-Al disordered distribution) or dynamic disorder (thermal motion), cause the observed interatomic distances to be shorter than the actual bond lengths, and he further hypothesized a correlation between the isotropic temperature factors of O atoms and the observed interatomic distances. Starting from these hypotheses, we also applied the method proposed by Alberti and Gottardi (1988) for framework silicates, duly adapted to layer silicate structures. The method provides satisfactory agreement with chemical analyses (Table 8). Figure 6, where t_{tet} is plotted against the $^{[4]}X_{Al}$ [X_{Al} = $^{[4]}$Al/($^{[4]}$Al + $^{[4]}$Si)], clearly shows that the tetrahedral sheet thickness decreases as $^{[4]}$Al content increases.

Figures 7a and 7b, where the mean distance ⟨T-O⟩ is plotted vs. ⟨M1-O⟩ and ⟨M2-O⟩, respectively, show that

TABLE 8. Determination of Al/(Al + Si) for the biotite samples

Sample	1	2	3	4
8	0.282	0.289	0.305	0.286
9	0.258	0.261	0.272	0.273
10	0.252	0.218	0.245	0.267
11	0.270	0.268	0.281	0.283
12	0.252	0.254	0.268	0.274
15	0.295	0.289	0.314	0.317
16	0.276	0.282	0.308	0.298
17	0.258	0.282	0.304	0.309

Note: For each sample the data were obtained according to: 1 = Hazen and Burnham (1973); 2 = Abbott and Burnham (1988); 3 = Alberti and Gottardi (1988); 4 = microprobe chemical analyses.

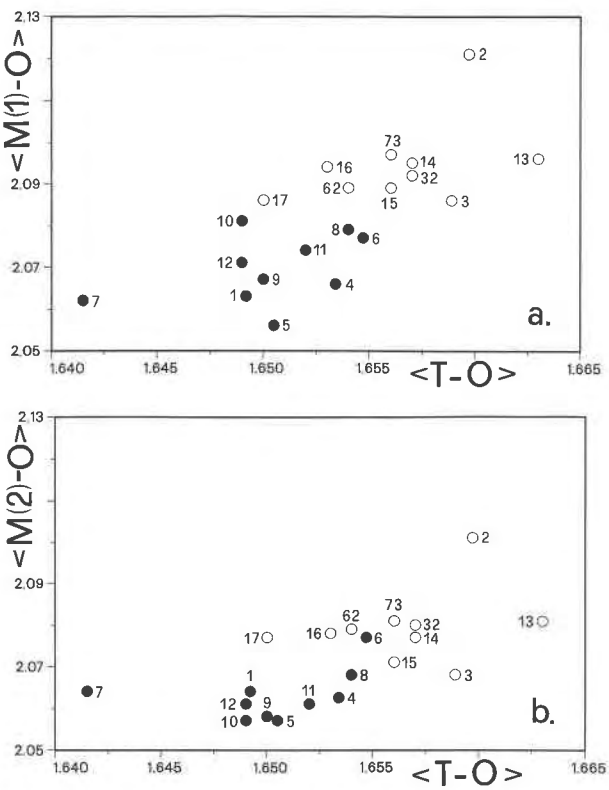

Fig. 7. Mean ⟨M-O⟩ distance (Å) vs. mean ⟨T-O⟩ distance (Å) for M1 (**a**) and M2 (**b**). Symbols and samples as in Figure 1.

an increase in octahedral dimensions causes an increase in those of the tetrahedra. Samples with $Mg/^{[6]}\Sigma > 0.5$ fall into an area that is distinct from those of samples with $Mg/^{[6]}\Sigma < 0.5$. These features are particularly evident when the mean distances of ⟨M1-O⟩ and ⟨T-O⟩ are compared.

If the dimensions of the octahedral and tetrahedral sheets are different, the linkage of the tetrahedra with octahedra M1 and M2 is allowed by variations in the rotation angle α (as defined by Newnham and Brindley, 1956 and as calculated in Hazen and Burnham, 1973) ($5.23 \leq \alpha \leq 7.97$; Table 6).

Summary and conclusions

In the trioctahedral micas, M1 and M2 octahedra have similar geometry (size and distortion) in Mg end-members. As Fe content, high-charge octahedral cations, or both increase, M1 and M2 octahedra become progressively more distinct both in size and distortion.

Although the octahedral sheet is characterized by a disordered cation distribution, the results of this study seem to indicate that in samples where $Mg/^{[6]}\Sigma > 0.5$, the M2 octahedra are similar in geometry to the M2 octahedra in end-member phlogopite. This may be a consequence of preferential ordering of Mg cations in M2 sites. No preferential ordering of octahedral cations seems to exist, however, when $Mg/^{[6]}\Sigma < 0.5$.

Ti^{4+} substitutes for Mg^{2+} or Fe^{2+} preferentially in the M1 site. In samples where $Mg/^{[6]}\Sigma > 0.5$, this substitution is partly balanced by octahedral vacancies and by substitution of Al for Si according to reactions

$$^{[6]}Ti + {}^{[6]}\square = 2\,{}^{[6]}(Fe,Mg)$$

$$^{[6]}Ti + 2\,{}^{[4]}Al = {}^{[6]}(Mg,Fe) + 2\,{}^{[4]}Si.$$

The tetrahedral sheet dimensions (thickness and mean distances) are not solely affected by Al → Si substitution but also by octahedral features.

Acknowledgments

We would like to thank T. Andersen, S. Capedri, K.L. Currie, and A. Rottura for making rock specimens available for investigation.

Thanks are due to R.N. Abbott and T.C. Labotka for their helpful suggestions and stylistic improvements.

Financial support was provided by Centro Calcolo and Centro Strumenti of Modena University, Ministero della Pubblica Istruzione and Consiglio Nazionale delle Ricerche of Italy. The Consiglio Nazionale delle Ricerche is also acknowledged for financing the Electron Microprobe Laboratory at Modena University.

References cited

Abbott, R.N., Jr., and Burnham, C.W. (1988) Polytypism in micas: A polyhedral approach to energy calculations. American Mineralogist, 73, 105–118.

Abrecht, J., and Hewitt, D.A. (1988) Experimental evidence on the substitution of Ti in biotite. American Mineralogist, 73, 1275–1284.

Albee, A.L., and Ray, L. (1970) Correction factors for electron microanalysis of silicates, oxides, carbonates, phosphates and sulphates. Analytical Chemistry, 42, 1408–1414.

Alberti, A., and Gottardi, G. (1988) The determination of the Al-content in the tetrahedra of framework silicates. Zeitschrift für Kristallographie, 184, 49–61.

Andersen, T. (1984) Crystallization history of a Permian composite monzonitic–alkali syenite pluton in the Sande cauldron, Oslo rift, southern Norway. Lithos, 17, 153–170.

Bailey, S.W. (1975) Cation ordering and pseudosymmetry in layer silicates. American Mineralogist, 60, 175–187.

——— (1984) Crystal chemistry of the true micas. In Mineralogical Society of America Reviews in Mineralogy, 13, 13–60.

Brigatti, M.F., and Davoli, P. (1990) Crystal-structure refinements of *1M* plutonic biotites. American Mineralogist, 75, 305–313.

Busing, W.R., Martin, K.O., and Levy, H.S. (1962) ORFLS, a Fortran crystallographic least-square program. U.S. National Technical Information Service, ORNL-TM-305.

Currie, K.L., Nelsonebi, G., and Gittings, J. (1986) The petrology of the Mont Saint Hilaire Complex, southern Quebec: An alkaline gabbro-peralkaline syenite association. Lithos, 19, 65–81.

Davoli, P. (1989) Reciprocal lattice scan modes in single crystal diffractometry: A re-examination for cases of mineralogical interest. Zeitschrift für Kristallographie, 188, 11–29.

Donnay, G., Donnay, J.D.H., and Takeda, H. (1964) Trioctahedral one-layer micas. II. Prediction of the structure from composition and cell dimensions. Acta Crystallographica, 17, 1374–1381.

Dymek, R.F. (1983) Titanium, aluminum and interlayer cation substitutions in biotite from high-grade gneisses, West Greenland. American Mineralogist, 68, 880–899.

Einstein, J.R. (1974) Analysis of intensity measurements of Bragg reflections with a single crystal equatorial plane diffractometer. Journal of Applied Crystallography, 7, 331–344.

Guidotti, C.V., Cheny, J.T., and Guggenheim, S. (1977) Distribution of titanium between coexisting muscovite and biotite in pelitic schists from northwestern Maine. American Mineralogist, 62, 438–448.

Hazen, R.M., and Burnham, C.W. (1973) The crystal structure of one-layer phlogopite and annite. American Mineralogist, 58, 889–900.

Hazen, R.M., Finger, L.W., and Velde, D. (1981) Crystal structures of a silica and alkali-rich trioctahedral mica. American Mineralogist, 66, 586–591.

Joswig, W. (1972) Neutronenbeugungsmessungen an einem 1M-phlogopit. Neues Jahrbuch Mineralogie Monatschefte, 1–11.

Labotka, T.C. (1983) Analysis of the compositional variations of biotite in pelitic hornfelses from northeastern Minnesota. American Mineralogist, 68, 900–914.

Liebau, F. (1985) Structural chemistry of silicates. Springer, Heidelberg.

McCauley, J.W., Newnham, R.E., and Gibbs, G.V. (1973) Crystal structure analysis of synthetic fluorophlogopite. American Mineralogist, 58, 249–254.

McKinney, J.A., Mora, C.I., and Bailey, S.W. (1988) Structure and crystal chemistry of clintonite. American Mineralogist, 73, 365–375.

Newnham, R.E., and Brindley, G.W. (1956) The crystal structure of dickite. Acta Crystallographica, 9, 759–764.

North, A.C.T., Phillips, D.C., and Mathews, F.S. (1968) A semi-empirical method of absorption correction. Acta Crystallographica, A24, 351–359.

Robinson, K., Gibbs, G.V., and Ribbe, P.H. (1971) Quadratic elongation, a quantitative measure of distortion in coordination polyhedra. Science, 172, 567–570.

Rottura, A., Bargossi, G.M., Caironi, V., Del Moro, A., Maccarrone, E., Macera, P., Paglionico, A., Petrini, R., Piccarreta, G., and Poli, G. (1990) Petrogenesis of contrasting Hercinian granitoids from the Calabrian Arc, southern Italy. Lithos, 24, 97–119.

Takeda, H., and Morosin, B. (1975) Comparison of observed and predicted structural parameters of mica at high temperature. Acta Crystallographica, B31, 2444–2452.

Takeda, H., and Ross, M. (1975) Mica polytypism: Dissimilarities in the crystal structures of coexisting 1M and $2M_1$ biotite. American Mineralogist, 60, 1030–1040.

Toraya, H. (1981) Distortions of octahedra and octahedral sheets in 1M micas and the relation to their stability. Zeitschrift für Kristallographie, 157, 173–190.

Vainshtein, B.K. (1981) Modern crystallography. I. Symmetry of crystals, methods of structural crystallography. Springer-Verlag, Berlin.

Venturelli, S., Capedri, S., Di Battistini, G., Crawford, A., Kogarko, L.N., and Celestini, S. (1984) The ultrapotassic rocks from southeastern Spain. Lithos, 17, 37–54.

Venturelli, G., Salvioli Mariani, E., Foley, S.F., Capedri, S., and Crawford, A.J. (1988) Petrogenesis and crystallization of Spanish lamproitic rocks. Canadian Mineralogist, 26, 67–79.

Weiss, Z., Rieder, M., Chmielová, M., and Krajicek, J. (1985) Geometry of the octahedral coordination in micas: A review of refined structures. American Mineralogist, 70, 747–757.

Ziebold, T.O., and Ogilvie, R.E. (1964) An empirical method for electron microanalysis. Analytical Chemistry, 36, 322–327.

Manuscript received April 5, 1990
Manuscript accepted March 15, 1991